Journal of Materials Chemistry

Cite this: *J. Mater. Chem.*, 2011, **21**, 18447

www.rsc.org/materials

PAPER

Hollow Pt-Ni alloy nanospheres with tunable chamber structure and enhanced activity†

Hui Li,*[a] Hong Lin,[a] Ying Hu,[a] Hexing Li,*[a] Ping Li[b] and Xinggui Zhou[b]

Received 7th April 2011, Accepted 13th July 2011
DOI: 10.1039/c1jm11461a

Hollow Pt-Ni alloy nanospheres with tunable chamber size and shell thickness are prepared through a modified galvanic replacement approach. The strategy for fabricating such hollow alloys is discussed based on systematic characterization. During the liquid-phase *p*-chloronitrobenzene hydrogenation to *p*-chloroaniline, these hollow alloy materials exhibit much higher activity, greatly enhanced selectivity and better durability than the solid Pt nanoparticles. Of particular interest is the controllable shell thickness, which allows for tuning of catalytic activity.

Introduction

The preparation of nanophase materials with controllable morphology has been the focus of intense study in materials, because materials with unique shapes always exhibit fascinating functions and enhanced properties.[1] Recently, hollow materials with tunable chamber have captured increasing attention because of their potential applications in catalysis, adsorption, microelectronics, and photonics *etc.*[2] Among various hollow materials, hollow metal nanospheres represent a kind of new powerful catalyst owing to their increased surface area, low density, easy recovery, self-supporting capacity, cost reduction, and surface permeability compared with their solid counterparts.[3] Such special hollow structures in metals is routinely fabricated by using a soft-templating or hard-templating method. The soft templating method is generally used to coat metals onto the surface of vesicles or emulsion droplets by an interfacial reduction strategy. However, the fabrication of hollow metal spheres with tunable inner and outer diameters is not easy, due to the "soft" nature of the structuring units and the difficulty in controlling the phase behavior of surfactants. The hard templating method is usually used to deposit metals onto the surface of "hard" templates (*e.g.*, polymer colloid beads and silica spheres) *via* a layer-by-layer technique, which shows advantages over the soft-templating method in transcriptive imprinting of the template morphology and finely tuning the chamber size and shell thickness of hollow metal spheres.[3d–f] However, this approach involves the deposition of metal and the subsequent template removal, complicating the preparation process. From the viewpoint of practical applications, exploring more facile approaches to preparing hollow metal nanospheres with tunable chamber size and shell thickness, especially in large scale production, is an important issue.

In 2002, Xia's group reported a one-step approach to preparing hollow metallic nanospheres through a galvanic replacement method,[4] which is more facile and cost-effective since the template could act as a reducing agent to produce the metal shell and no additional steps are needed to remove the template. Henceforth, a series of hollow metals with tunable interior-cavity sizes have been synthesized by using Ag or Co nanoparticles as sacrificial templates.[5] However, the synthesis of hollow metallic nanospheres is limited mainly to noble metals by this synthesis strategy and thus their practical applications are limited due to the high cost. It is well recognized that binary alloys consisting of a noble metal and a non-noble metal could reduce the catalyst cost and effectively tailor the catalytic performances since the non-noble metal can mediate both the structural and the electronic properties of the noble metal.[6] In the case of chemoselective hydrogenation of substituted nitroaromatics to the corresponding substituted anilines, for instance, one of the most promising approaches to improving selectivity is modifying noble metals by alloying them with non-noble metals.[7]

Recently, Schaak's group successfully synthesized hollow CoPt alloy nanospheres through a modified galvanic replacement, which has been demonstrated to be a good superparamagnetic material.[8] However, the adjustment of the interior structure in such hollow alloys was never addressed, which may be important for tuning the catalytic performance. By using Ni nanoparticles with tunable size as sacrificial templates, herein we synthesize hollow Pt-Ni alloy nanospheres with controllable

[a]*Department of Chemistry and The Education Ministry Key Lab of Resource Chemistry, Shanghai Normal University, Shanghai, 200234, China. E-mail: lihui@shnu.edu.cn; hexing-li@shnu.edu.cn; Fax: +86-21-64322272; Tel: +86-21-64322642*
[b]*State Key Laboratory of Chemical Engineering, East China University of Science and Technology, Shanghai, 200237, China*

† Electronic Supplementary Information (ESI) available: TEM images of the sample taken after reaction 4 min during the preparation of Pt-Ni-50 (H), Ni nanoparticles template for the preparation of Pt-Ni-50(H), Pt-Ni sample synthesized in the presence of high amount of PVP (150 mg), Pt-Ni sample synthesized by using the Ni nanoparticles without PVP as templates, and Pt-Ni sample synthesized with the molar ratio of Pt to Ni of 1/2. See DOI: 10.1039/c1jm11461a/

chamber size and shell thickness. Their catalytic properties are investigated in liquid-phase *p*-chloronitrobenzene (*p*-CNB) hydrogenation to *p*-chloroaniline (*p*-CAN), which is an important product for pharmaceuticals, pesticides and dyes.[9] Experimental results demonstrate that the Pt-Ni alloy is superior to the individual Pt. Furthermore, the hollow chamber also exerts a promotional effect on the catalytic activity, and thus the catalytic activity of hollow Pt-Ni alloy nanospheres can be tuned by controlling the interior-cavity size and shell thickness.

Experimental

Material preparation

All chemicals used in this experiment were analytical grade and used without further purification. Hollow Pt-Ni alloy nanospheres are prepared according to the following galvanic displacement method. First, $NiCl_2 \cdot 6H_2O$ (34.0 mg, 0.143 mmol) and poly(vinylpyrrolidone) (PVP; MW = 40 000) of desired weight are dissolved in deaerated ultrapure H_2O (200 mL) in a three-necked flask and maintained at 293 K under vigorous stirring. The mixture is sonicated for 15 min and purged with high-purity argon for 15 min. Then, 80 mL of $NaBH_4$ (40.0 mg, 1.06 mmol) aqueous solution is added dropwise into the above solution under vigorous stirring at 293 K. Immediately after all of the $NaBH_4$ has been added, 80 mL of K_2PtCl_6 (65.6 mg, 0.135 mmol) aqueous solution is added dropwise at a rate of 5.0 mL min^{-1}. To avoid the oxidation of the products in the existence of atmospheric oxygen, high-purity Ar is bubbled through the reaction system during the whole procedure. After 30 min, the black precipitate is washed thoroughly with H_2O until the pH reaches 7, followed by washing with ethanol (EtOH) three times, and dried under ambient conditions. The as-prepared Pt-Ni samples are denoted as Pt-Ni-*x*(H), where *x* refers to the amount of PVP (mg). For comparison, solid Ni and Pt samples are also synthesized by direct reduction of Ni^{2+} or $PtCl_6^{2-}$ with BH_4^-, and are denoted as Ni(S) and Pt(S), respectively. Briefly, Ni(S) is prepared by chemical reduction of 200 mL of $NiCl_2 \cdot 6H_2O$ (34.0 mg, 0.143 mmol) aqueous solution with 40 mL of $NaBH_4$ (20.0 mg, 0.530 mmol) aqueous solution under vigorous stirring at 293 K. Pt(S) is prepared by chemical reduction of 100 mL of K_2PtCl_6 (65.6 mg, 0.135 mmol) aqueous solution with 20 mL of $NaBH_4$ (10.0 mg, 0.265 mmol) aqueous solution under vigorous stirring at 293 K.

Catalyst characterization

The bulk composition is analyzed by inductively coupled plasma-optical emission spectroscopy (ICP-OES; Varian VISTA-MPX). Fourier transform infrared (FTIR) spectra are recorded on a Nicolet Magna 550 spectrometer by the KBr technique. The crystalline structure is determined by X-ray powder diffraction (XRD; Rigaku Dmax-3C). The catalyst shapes and morphologies are observed through transmission electron microscopy (TEM; JEOL JEM2100). The diameter and shell thickness distributions are evaluated from about 300 randomly selected particles. The surface electronic states are investigated by X-ray photoelectron spectroscopy (XPS; ULVAC-PHI PHI 5000 VersaProbe). All the binding energies (BE) are calibrated by using the contaminant carbon (C 1*s* = 284.6 eV) as a reference. N_2 adsorption–desorption isotherms are obtained on a Quantachrome Nova 4000e analyzer at 77 K. Surface active areas (S_{Pt}) are measured by hydrogen chemisorption on a Quantachrome ChemBET-3000 system assuming H/M(S) = 1. The atomic cross section of Pt is taken as 9.84×10^{-20} m^2. For bimetallic catalysts, only hydrogen adsorption on Pt is considered for the calculation of S_{Pt}. Thus, the hydrogen adsorption on Ni is removed from the total hydrogen uptake on the basis of surface concentration measured by XPS analysis.[10]

Activity measurement

Liquid-phase *p*-CNB hydrogenation is performed in a three-necked flask. A catalyst containing 0.132 mmol of Pt, 20 mmol of *p*-CNB, and 50 mL of EtOH are introduced into the reactor. High purity, oxygen-free hydrogen gas is bubbled through the mixture at atmosphere pressure with a rate of 80 mL min^{-1}. After the apparatus is flushed with hydrogen at room temperature for 30 min, the reaction mixture is vigorously agitated (800 rpm) throughout the catalytic run by a magnetic stirrer bar and maintained at 303 K. A condenser is attached to the hydrogen exit to prevent solvent loss. The reaction mixture is sampled at intervals for product analysis through a gas chromatograph (GC) equipped with a flame ionization detector (FID) and an AC-5 column by using *n*-$C_{12}H_{25}OH$ as internal standard, from which reaction conversion and selectivity are calculated. The GC conditions are as follows: injector temperature, 513 K; oven temperature, programmed from 373 to 513 K at a ramping rate of 15 K min^{-1}; carrier gas N_2, 30 mL min^{-1}. Reproducibility was checked by repeating the runs at least three times and was found to be within acceptable limits (±5%).

Results and discussion

Material characterization

The FTIR spectra (Fig. 1) demonstrate the adsorption of PVP molecules on the Pt-Ni(H) sample, corresponding to the C=O stretching vibration around 1656 cm^{-1},[11] the C–N bond stretching vibration at 1286 cm^{-1},[12] as well as the asymmetric

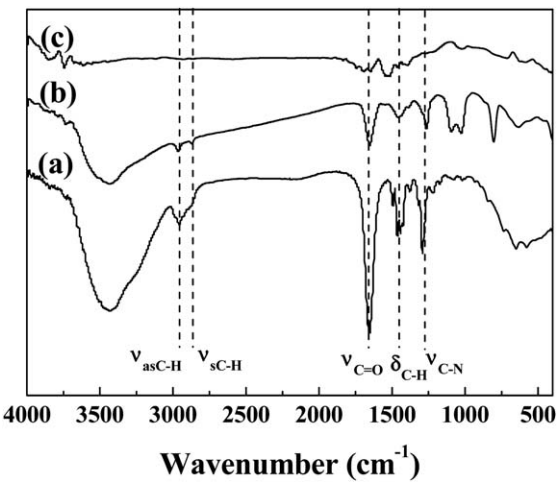

Fig. 1 FTIR spectra of (a) PVP, and Pt-Ni-50(H) (b) before and (c) after being washed.

stretching, symmetric stretching, and bending vibrations of aliphatic C–H around 2962, 2868, and 1447 cm^{-1}.[13] After being washed, these absorbance bands indicative of PVP molecular disappear completely, indicating the successful removal of the applied PVP capping reagent.

The TEM images in Fig. 2 demonstrate that the Ni(S) and Pt (S) samples are present in the form of solid particle. Ni(S) displayed almost shapeless particles with extremely broad size distribution (from <10 nm to >300 nm), apparently due to severe agglomeration.[14] The average size of Pt(S) is around 8 nm. The attached high resolution transmission electron microscopy (HRTEM) images reveal that the Pt(S) exhibits a typical face-centered cubic (fcc) Pt structure, corresponding to the Pt (111) interplanar space of 0.225 nm. Fig. 3 demonstrate that all the Pt-Ni-*x*(H) samples are present in the form of hollow nanospheres. The attached high-magnification TEM images reveal that the outer shells are composed of uniform nanoparticles. Meanwhile, wormhole-like mesopores in the outer shells can be clearly seen from the attached higher-magnification TEM images. The attached HRTEM images display that the Pt (111) interplanar spaces shift negatively to 0.218 nm in all Pt-Ni-*x*(H) samples, obviously owing to the incorporation of Ni atoms into the Pt lattice. With the increase of the amount of PVP from 10 to 100 mg, the average diameter of hollow nanospheres decreases from 350 to 7 nm, together with the decrease in shell thickness from 22 to 1.8 nm. It should be noted that, due to the very low density and colloidal properties of Pt-Ni-100(H) sample, there exists major difficulties in separating them from solution. Thus, other characterizations will not be performed on Pt-Ni-100(H) in the following studies.

XRD patterns (Fig. 4) reveal that Pt(S) and Ni(S) has an fcc structure and an amorphous structure, respectively. For all Pt-Ni-*x*(H), the diffraction peaks in the range $30 < 2\theta$ 80° could be indexed as fcc Pt (111), (200), and (220) (JCPDS 04-0802),[15] in good agreement with the above-mentioned HRTEM images. In comparison with the pure Pt, the diffraction peaks of all the Pt-Ni-*x*(H) samples shift to higher angles, corresponding to the decrease in the *d* value of the Pt (111) plane from 0.227 to 0.219 nm. The elemental mapping image for a single Pt-Ni-50(H) sphere in Fig. 4 displays that the hollow sphere demonstrated by the aforementioned TEM images contains both Ni and Pt. Taking into account that no peak for Ni is observed on the XRD patterns of all Pt-Ni-*x*(H) samples, one can conclude the formation of Pt-Ni alloy through the incorporation of Ni atoms into the Pt lattice.[16] The diffraction peaks for all the Pt-Ni-*x*(H) samples are fairly broad, indicating the property of nanocrystals

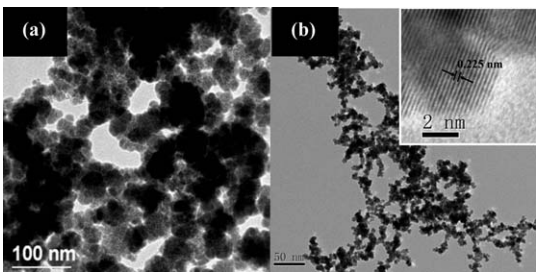

Fig. 2 Representative TEM images of (a) Ni(S) and (b) Pt(S). The insets are the corresponding HRTEM images.

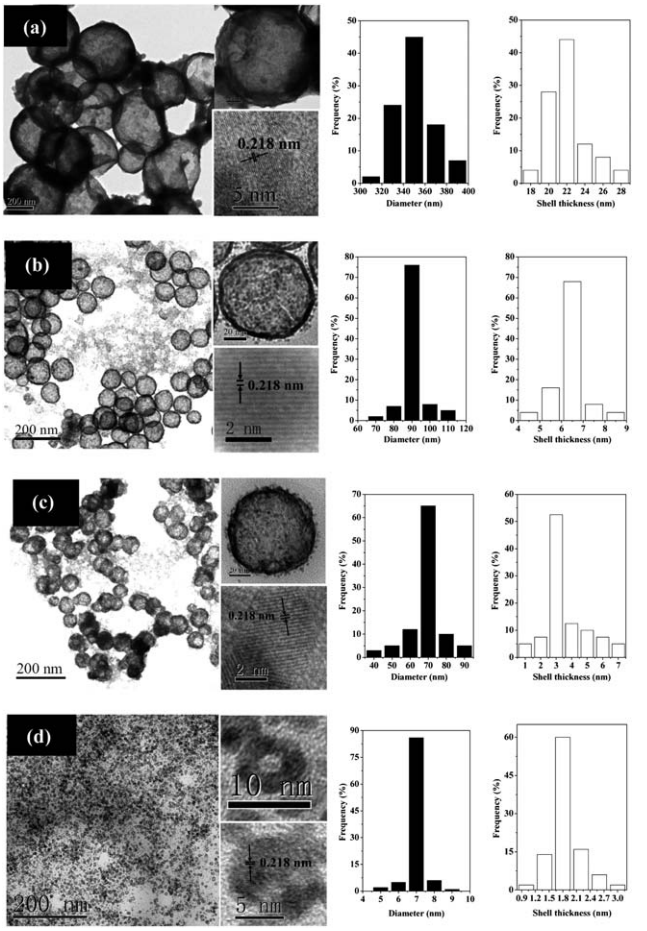

Fig. 3 Representative TEM images of (a) Pt-Ni-10(H), (b) Pt-Ni-25(H), (c) Pt-Ni-50(H), and (d) Pt-Ni-100(H). Also shown are the high-magnification TEM images, the HRTEM images, and distribution histograms of the diameter and the shell thickness.

(as confirmed by the small shell thickness). Meanwhile, the line broadening of the (111) reflection for Pt-Ni-*x*(H) can be further intensified by decreasing the sphere diameter (from Fig. 4b to d), which is most likely related to the decrease of shell thickness.

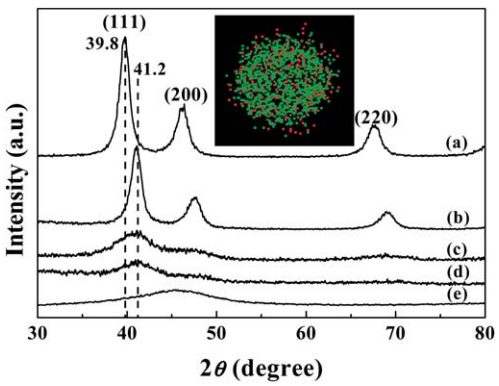

Fig. 4 XRD patterns of (a) Pt(S), (b) Pt-Ni-10(H), (c) Pt-Ni-25(H), (d) Pt-Ni-50(H), and (e) Ni(S). The inset shows the elemental mapping of Pt-Ni-50(H), indicating that the hollow sphere contains both Ni (red) and Pt (green).

The XPS spectra (Fig. 5) reveal that the Pt species in all the Pt-Ni-*x*(H) samples are present in the metallic state, corresponding to the BE around 71.6 and 74.8 eV in the Pt $4f_{7/2}$ and Pt $4f_{5/2}$ levels, respectively.[17] Meanwhile, all the Ni species are also proven to be present in the metallic state with the BE around 852.3 eV in the Ni $2p_{3/2}$ level.[18] In comparison with the BE values of pure Pt (71.2 eV) and pure Ni (853.1 eV), the BE of the Pt $4f_{7/2}$ level shifts positively while the BE of the Ni $2p_{3/2}$ level shifts negatively after forming Pt-Ni alloys. This indicates that partial electrons transfer from Pt to Ni, as demonstrated by Toda and Liu.[18] As a result, the combined results from HRTEM, XRD and XPS characterization clearly demonstrate the formation of Pt-Ni alloy through the present preparation method. The surface compositions of all the Pt-Ni-*x*(H) samples ($Comp^S$) are calculated from the relative peak areas in the XPS spectra, which are in good accordance with those determined by ICP analysis ($Comp^B$) (see Table 1).

Fig. 6 demonstrates that all the Pt-Ni-*x*(H) samples display type IV nitrogen adsorption–desorption isotherms with a hysteresis loop, indicative of mesoporous character. This can be attributed to the piling-up of the Pt-Ni alloy nanoparticles, as observed in the above-mentioned high-magnification TEM images. The active surface areas (S_{Pt}) are determined by hydrogen chemisorption. As shown in Table 1, the S_{Pt} of Pt-Ni-*x*(H) change in the order of Pt-Ni-50(H) > Pt-Ni-25(H) > Pt-Ni-10(H), obviously owing to the decrease in the shell thickness.

Formation process

The synthesis of hollow Pt-Ni alloy nanospheres through the modified galvanic displacement is designed on the basis of the redox reactions as follows

$$BH_4^- + 2Ni^{2+} + 2H_2O \rightarrow 2Ni + BO_2^- + 4H^+ + 2H_2 \quad (1)$$

$$BH_4^- + PtCl_6^{2-} + 2H_2O \rightarrow Pt + 6Cl^- + BO_2^- + 4H^+ + 2H_2 \quad (2)$$

$$2Ni + PtCl_6^{2-} \rightarrow Pt + 2Ni^{2+} + 6Cl^- \quad (3)$$

Firstly, Ni nanoparticle templates are fabricated through chemical reduction of Ni^{2+} ions with borohydride, reaction (1). The surface of the as-made Ni nanoparticles is wrapped with PVP, which acts as a stabilizer to protect Ni nanoparticles from agglomerating. When $PtCl_6^{2-}$ aqueous solution is added, a portion of $PtCl_6^{2-}$ ions are reduced by the excess BH_4^-, reaction (2). The produced Pt atoms will preferentially adsorb on the surface of PVP to reduce their surface energy. Meanwhile, partial $PtCl_6^{2-}$ ions can diffuse readily through the solution to arrive at the surface of Ni nanoparticles. As the standard reduction potential of the $PtCl_6^{2-}$/Pt pair (0.735 V *vs.* standard hydrogen electrode, SHE) is much higher than that of the Ni^{2+}/Ni pair (−0.25 V *vs.* SHE), $PtCl_6^{2-}$ ions are immediately reduced to Pt atoms by Ni, reaction (3).[5b] Once the Ni nanoparticles are sacrificially dissolved, the produced Ni^{2+} ions are trapped by the PVP surrounding on Ni nanospheres and re-reduced to Ni atoms by BH_4^-, reaction (1).[8] Because Pt and Ni nucleation sites are highly reactive, they diffuse quickly to form homogeneous bimetal in an alloy phase,[19] and eventually evolve into a shell around the original Ni core (Scheme 1A).[5a] The continuous reactions lead to the enhanced thickness of the Pt-Ni alloy shell and the consumption of the Ni core, until the formation of hollow Pt-Ni alloy spheres. This ecto-entad stepwise replacement process can be demonstrated by the observation of core–shell nanospheres in the initial stage of preparation (Fig. S1†). Herein, the Ni core provides an *in situ* template for the deposition of Pt-Ni alloys. Obviously, the interior-cavity size of the final product is almost the same as the diameter of the Ni nanoparticle template (Fig. S2†). Adjusting the amount of PVP can easily tune the diameter of Ni nanoparticles, and thus determine definitely the interior-cavity size of hollow Pt-Ni nanospheres (Fig. 3). In addition, the shell thickness is also strongly dependent on the size of the original Ni core (Fig. 3). The larger the Ni nanoparticles diameter, the thicker the shells will be, owing to the formation of more overlapped Pt-Ni alloys. Besides adjusting the size of Ni cores, PVP also plays a key role in the formation of Pt-Ni alloy phases. By using Ni nanoparticles without PVP, a mixture of hollow, core–shell structured and solid particles is obtained (Fig. S4†). EDX analysis confirmed that the solid particles are comprised of pure Pt rather than Pt-Ni alloy. Due to the absence of PVP, most of the produced Pt atoms reduced by BH_4^- are not easily bound to the surface of Ni cores, and finally grow into Pt nanoparticles during solution (Scheme 1B). Furthermore, the amount of $PtCl_6^{2-}$ ions also significantly influences the formation of hollow Pt-Ni alloy nanospheres. According to the replacement reaction between Ni and $PtCl_6^{2-}$, reaction (3), the theoretical molar ratio of Pt to Ni is 1/2. However, only a sample with core–shell structure is obtained with such molar ratio of reactants (Fig. S5†), due to the incomplete consumption of the Ni core (Scheme 1C). Doubling the amount of K_2PtCl_6 results in the formation of hollow alloy with a composition of $Pt_{63}Ni_{37}$, accompanied with enhanced shell thickness (Fig. S6†). Obviously, the Pt/Ni molar ratio in the hollow Pt-Ni sample could be regulated to some degree.

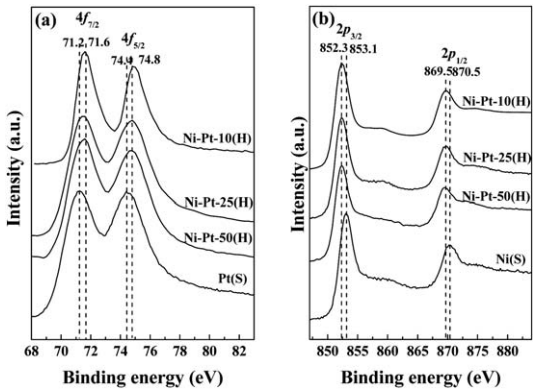

Fig. 5 XPS spectra of (a) Pt 4*f* and (b) Ni 2*p* in different samples.

Catalysis performance

The liquid phase *p*-CNB hydrogenation to *p*-CAN under atmospheric pressure and 303 K is used for evaluating the performances of the as-prepared catalysts. Fig. 7 shows the concentration change of both the reactant and the products with the reaction time during *p*-CNB hydrogenation over Pt-Ni-50(H). Except for the main product *p*-CAN, only aniline (AN)

Table 1 Some structural and catalytic parameters of the as-prepared catalysts[a]

Catalyst	Comp[B] (atom%)	Comp[S] (atom%)	S_{Pt} (m^2 g^{-1})	TOF (s^{-1})	Conversion (%)	Selectivity (%)	Reaction time (min)
Pt(S)	Pt	Pt	7.1	0.56	97	76	200
Pt-Ni-10(H)	$Pt_{48}Ni_{52}$	$Pt_{47}Ni_{53}$	8.5	0.62	99	97	70
Pt-Ni-25(H)	$Pt_{45}Ni_{55}$	$Pt_{49}Ni_{51}$	11	0.62	99	99	50
Pt-Ni-50(H)	$Pt_{47}Ni_{53}$	$Pt_{48}Ni_{52}$	14	0.64	99	98	40

[a] *Reaction conditions*: a catalyst containing 0.132 mmol of Pt, 20 mmol of *p*-CNB, 50 mL of EtOH, $T = 303$ K, $P_{H2} = 1.0$ atm, stirring rate = 800 rpm.

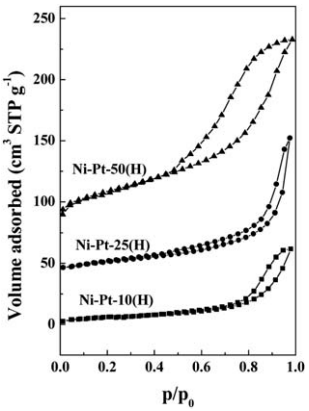

Fig. 6 Adsorption/desorption isotherms of Pt-Ni-*x*(H).

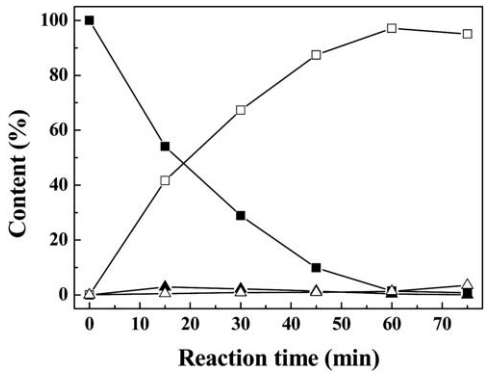

Fig. 7 Hydrogenation of *p*-CNB over Pt-Ni-50(H) catalyst as a function of reaction time. (■) *p*-CNB, (□) *p*-CAN, (▲) NB, (△) AN. Reaction conditions are listed in Table 1.

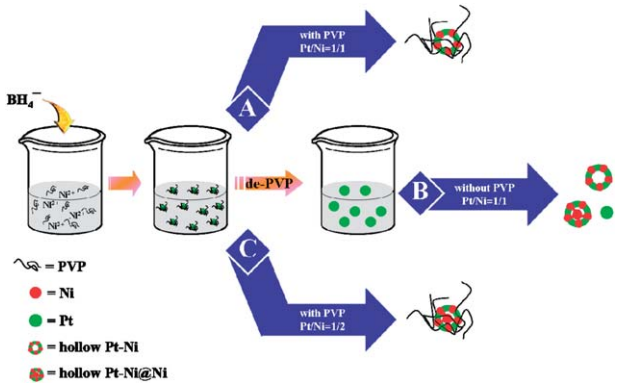

Scheme 1 Formation process of hollow Pt-Ni alloys.

and nitrobenzene (NB) are identified as by-products under the present conditions, suggesting that the *p*-CNB hydrogenation follows the pathways described in Scheme 2.[20] Ni(S) does not show any catalytic activity under the present conditions, indicating platinum is the active sites.

Table 1 summarizes some structural and catalytic parameters of different catalysts. Catalytic parameters include the turnover frequency (TOF, the number of *p*-CNB molecule converted per second per surface Pt site), the conversion and the selectivity to *p*-CAN obtained at the maximum *p*-CAN yield, together with the time needed to reach the maximum *p*-CAN yield. Based on the reaction time, it is obvious that all the Pt-Ni-*x*(H) samples exhibit much higher activity than the pure Pt(S). This could be attributed to the enhanced dispersion degree of Pt active sites (S_{Pt}) and the increased intrinsic activity (TOF). The larger S_{Pt} of Pt-Ni-*x*(H) compared to Pt(S) can be interpreted in terms of the promotional effect of both the chamber structure and the alloying Ni. Such hollow structure could increase the accessibility and provide much more active sites, while the dispersing effect of Ni-dopant on Pt active sites is apparently favorable for hydrogenation. Besides the enhanced S_{Pt}, Pt-Ni-*x*(H) exhibit increased intrinsic activity relative to Pt(S). As identified by XPS results, the Pt in Pt-Ni alloys is more electron deficient than pure Pt owing to the electron donation from Pt to Ni. Such electron-deficient Pt active sites favor the dissociative adsorption of hydrogen molecules to form $H^{\delta-}$,[21] leading to the enhanced activity because the nucleophilic attack of $H^{\delta-}$ on the nitrogen atom of the nitro group is a rate-determining step of *p*-CNB hydrogenation.[22] In addition, all the Pt-Ni-*x*(H) samples are also more selective towards *p*-CAN than Pt(S), since the electron-deficient Pt active sites can "recognize" and preferentially adsorb the electron-enriched nitro group.[7b] Accordingly, the dehalogenation reaction is efficiently retarded, leading to higher *p*-CAN selectivity. For Pt-Ni-*x*(H) samples, the reactivity can be intensified by decreasing the diameter of the hollow nanospheres, obviously owing to the decrease in the shell thickness and thus the increase in S_{Pt}. The

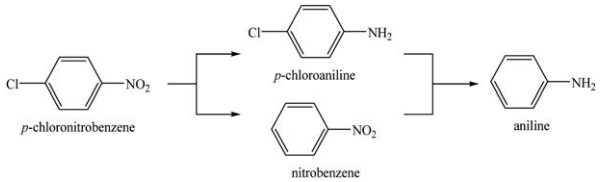

Scheme 2 Plausible route of *p*-CNB hydrogenation.

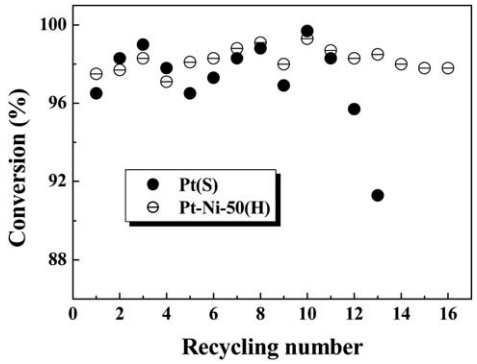

Fig. 8 Recycling test in liquid-phase *p*-CNB hydrogenation. Reaction conditions are given in Table 1.

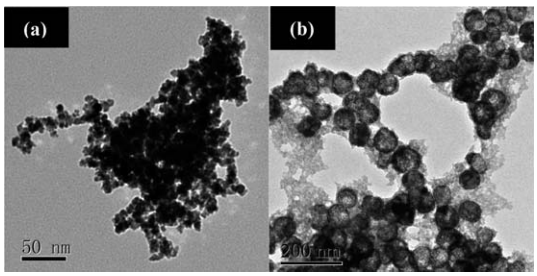

Fig. 9 TEM images of (a) Pt(S) and (b) Pt-Ni-50-(H) after 13 and 16 consecutive runs, respectively.

maximum hydrogenation conversion is obtained on Pt-Ni-50(H), and is about 5 times that on Pt(S).

Stability studies

Fig. 8 shows the recycling tests of Pt(S) and Pt-Ni-50(H). The *p*-CNB conversions decrease by 5.4% on Pt(S) after being used 13 times. However, Pt-Ni-50(H) can be used repetitively more than 16 times without significant loss of activity. ICP analysis detected that the weight loss of Pt(S) after 13 consecutive runs is 2.1%; while no leaching of Pt could be detected for Pt-Ni-50(H) during repetitive uses. This implies that the loss of catalyst during recycling tests is one factor responsible for the deactivation of Pt(S). Because of the large diameter of hollow nanospheres, Pt-Ni-50(H) can be easily separated from solution *via* centrifugation, which diminishes the loss of catalyst during recycling tests.[3g] In addition, TEM images (Fig. 9) reveal that the deactivation of Pt(S) can be also due to a severe agglomeration of nanoparticles. However, the hollow chamber of Pt-Ni-50(H) is quite stable which can be well preserved after being used 16 times (Fig. 9b). According to this observation, the high durability of Pt-Ni-50(H) can also be attributed to its self-supporting capacity, which retards the Pt-Ni nanoalloys from agglomeration during the hydrogenation process.[3g]

Conclusions

In summary, hollow Pt-Ni alloy nanospheres have been successfully synthesized through a facile galvanic replacement method by using Ni nanoparticles as sacrificial templates. The chamber structure with alloying shell has been shown to have a positive influence on the catalytic behavior in the liquid-phase *p*-CNB hydrogenation to *p*-CAN. Moreover, these hollow nanospheres have tunable chamber size and shell thickness, which provides a level of reactivity control. By the present method, it is possible to create other hollow nanospheres with different sizes and different alloying compositions for designing novel and powerful catalysts.

Acknowledgements

This work is supported by the National Natural Science Foundation of China (20973113, 20825724), the 973 Project (2009CB226106), and Shanghai Government (09JC1411400, 10SG41, S30406, 07dz22303), and State Key Laboratory of Chemical Engineering (SKL-ChE-09C03).

Notes and references

1 (*a*) Y. F. Lu, H. Y. Fan, A. Stump, T. L. Ward, T. Rieker and C. J. Brinker, *Nature*, 1999, **398**, 223; (*b*) J. T. Hu, T. W. Odom and C. M. Lieber, *Acc. Chem. Res.*, 1999, **32**, 435; (*c*) J. N. Cha, G. D. Stucky, D. E. Morse and T. J. Deming, *Nature*, 2000, **403**, 289.
2 (*a*) Y. Sun, B. Mayers and Y. Xia, *Adv. Mater.*, 2003, **15**, 641; (*b*) Y. Song, R. M. Garcia, R. M. Dorin, H. Wang, Y. Qiu and J. A. Shelnutt, *Angew. Chem., Int. Ed.*, 2006, **45**, 8126; (*c*) H. X. Li, Z. F. Bian, J. Zhu, D. Q. Zhang, G. S. Li, Y. N. Huo, H. Li and Y. F. Lu, *J. Am. Chem. Soc.*, 2007, **129**, 8406; (*d*) H. Xu and W. Wang, *Angew. Chem., Int. Ed.*, 2007, **46**, 1489.
3 (*a*) Y. Li, P. Zhou, Z. Dai, Z. Hu, P. Sun and J. C. Bao, *New J. Chem.*, 2006, **30**, 832; (*b*) P. Zhou, Y. Li, P. Sun, J. Zhou and J. C. Bao, *Chem. Commun.*, 2007, 1418; (*c*) G. Chen, D. Xia, Z. Nie, Z. Wang, L. Wang, L. Zhang and J. Zhang, *Chem. Mater.*, 2007, **19**, 1840; (*d*) S. W. Kim, M. Kim, W. Y. Lee and T. Hyeon, *J. Am. Chem. Soc.*, 2002, **124**, 7642; (*e*) X. Chen, W. Yang, S. Wang, M. Qiao, S. Yan, K. Fan and H. He, *New J. Chem.*, 2005, **29**, 266; (*f*) F. Cheng, H. Ma, Y. Li and J. Chen, *Inorg. Chem.*, 2007, **46**, 788; (*g*) H. Li, J. Liu, S. Xie, M. Qiao, W. Dai, Y. Lu and H. X. Li, *Adv. Funct. Mater.*, 2008, **18**, 3235; (*h*) H. Li, Z. H. Zhu, J. Liu, S. H. Xie and H. X. Li, *J. Mater. Chem.*, 2010, **20**, 4366; (*i*) H. Li, D. Q. Zhang, G. S. Li, Y. Xu, Y. F. Lu and H. X. Li, *Chem. Commun.*, 2010, **46**, 791.
4 Y. Sun and Y. Xia, *Science*, 2002, **298**, 2176.
5 (*a*) Y. Sun, B. T. Mayers and Y. Xia, *Nano Lett.*, 2002, **2**, 481; (*b*) H. P. Liang, H. M. Zhang, J. S. Hu, Y. G. Guo, L. J. Wan and C. L. Bai, *Angew. Chem., Int. Ed.*, 2004, **43**, 1540; (*c*) H. P. Liang, Y. G. Guo, H. M. Zhang, J. S. Hu, L. J. Wan and C. L. Bai, *Chem. Commun.*, 2004, 1496; (*d*) H. P. Liang, L. J. Wan, C. L. Bai and L. Jiang, *J. Phys. Chem. B*, 2005, **109**, 7795.
6 R. Ferrando, J. Jellinek and R. L. Johnston, *Chem. Rev.*, 2008, **108**, 845.
7 (*a*) B. Coq, A. Tijani and F. Figuéras, *J. Mol. Catal.*, 1992, **71**, 317; (*b*) A. Corma, P. Serna, P. Concepción and J. J. Calvino, *J. Am. Chem. Soc.*, 2008, **130**, 8748.
8 Y. Vasquez, A. K. Sra and R. E. Schaak, *J. Am. Chem. Soc.*, 2005, **127**, 12504.
9 E. Thomas and J. Nickson, *J. Org. Chem.*, 1986, **51**, 3903.
10 A. Tanksale, J. N. Beltramini, J. A. Dumesic and G. Q. Lu, *J. Catal.*, 2008, **258**, 366.
11 E. Hao and T. Lian, *Langmuir*, 2000, **16**, 7879.
12 Y. Borodko, S. E. Habas, M. Koebel, P. Yang, H. Frei and G. A. Somorjai, *J. Phys. Chem. B*, 2006, **110**, 23052.
13 A. S. Maria Chong and X. S. Zhao, *J. Phys. Chem. B*, 2003, **107**, 12650.
14 H. Li, J. Zhang and H. X. Li, *Catal. Commun.*, 2007, **8**, 2212.
15 T. C. Deivaraj, W. Chen and J. Y. Lee, *J. Mater. Chem.*, 2003, **13**, 2555.
16 K. W. Park, J. H. Choi, B. K. Kwon, S. A. Lee and Y. E. Sung, *J. Phys. Chem. B*, 2002, **106**, 1869.
17 Y. S. Lee, K. Y. Lim, Y. D. Chung, C. N. Whang and Y. Jeon, *Surf. Interface Anal.*, 2000, **30**, 475.

18 (*a*) T. Toda, H. Igarashi, H. Uchida and M. Watanabe, *J. Electrochem. Soc.*, 1999, **146**, 3750; (*b*) F. Liu, J. Y. Lee and W. Zhou, *J. Phys. Chem. B*, 2004, **108**, 17959.
19 X. Zhang and D. Li, *Angew. Chem., Int. Ed.*, 2006, **45**, 5971.
20 B. Coq, A. Tijani and F. Figuéras, *J. Mol. Catal.*, 1991, **68**, 331.
21 S. Yoshita, H. Yamashita, T. Funabiki and T. Yonezawa, *J. Chem. Soc., Faraday Trans. 1*, 1984, **80**, 1435.
22 P. Lu and N. Toshima, *Bull. Chem. Soc. Jpn.*, 2000, **73**, 751.